AGU PUBLICATIONS

JGR

Journal of Geophysical Research: Space Physics

RESEARCH ARTICLE

10.1002/2014JA020773

Key Points:
- Long-term records of geomagnetic data are statistically analyzed
- Equatorial electrojet response to geomagnetic storms and substorms is examined
- Dependence on longitude, storm magnitude, solar activity, and season is found

Correspondence to:
Y. Yamazaki,
y.yamazaki@lancaster.ac.uk

Citation:
Yamazaki, Y., and M. J. Kosch (2015), The equatorial electrojet during geomagnetic storms and substorms, *J. Geophys. Res. Space Physics*, *120*, doi:10.1002/2014JA020773.

Received 27 OCT 2014
Accepted 10 FEB 2015
Accepted article online 16 FEB 2015

The equatorial electrojet during geomagnetic storms and substorms

Yosuke Yamazaki[1] and Michael J. Kosch[1,2]

[1]Department of Physics, University of Lancaster, Lancaster, UK, [2]South African National Space Agency, Hermanus, South Africa

Abstract The climatology of the equatorial electrojet during periods of enhanced geomagnetic activity is examined using long-term records of ground-based magnetometers in the Indian and Peruvian regions. Equatorial electrojet perturbations due to geomagnetic storms and substorms are evaluated using the disturbance storm time (*Dst*) index and auroral electrojet (*AE*) index, respectively. The response of the equatorial electrojet to rapid changes in the *AE* index indicates effects of both prompt penetration electric field and disturbance dynamo electric field, consistent with previous studies based on *F* region equatorial vertical plasma drift measurements at Jicamarca. The average response of the equatorial electrojet to geomagnetic storms ($Dst < -50$ nT) reveals persistent disturbances during the recovery phase, which can last for approximately 24 h after the *Dst* index reaches its minimum value. This "after-storm" effect is found to depend on the magnitude of the storm, solar EUV activity, season, and longitude.

1. Introduction

During periods of elevated geomagnetic activity, equatorial ionospheric electric fields and currents undergo significant deviations from their quiet day patterns (e.g., *Fejer* [2002] for a review). Two mechanisms have been proposed to account for the generation of equatorial ionospheric electrodynamic effects for geomagnetically disturbed conditions. One is the prompt penetration of the high-latitude electric field to lower latitudes [*Nishida*, 1968; *Gonzales et al.*, 1979], and the other is the ionospheric dynamo due to storm time thermospheric winds [*Blanc and Richmond*, 1980]. Simulation studies have shown that electric field perturbations produced by these two processes can be comparable at equatorial latitudes [*Richmond et al.*, 2003; *Maruyama et al.*, 2005].

The prompt penetration of the high-latitude electric field is most evident when the magnetospheric convection suddenly increases or decreases. Under steady magnetospheric conditions, the inner magnetosphere tends to be shielded from the magnetospheric convection field [*Wolf*, 1995]. In other words, the middle- and low-latitude ionosphere is largely shielded from the effect of the high-latitude electric field. When the magnetospheric convection abruptly increases, the middle- and low-latitude ionosphere is exposed to the influence of the enhanced dawn-to-dusk convection electric field in the high-latitude ionosphere until the magnetospheric configuration readjusts and a new state of shielding is established. In contrast, a rapid decrease in the magnetospheric convection causes a temporary excess of the dusk-to-dawn shielding electric field, which affects lower latitudes until a reestablishment of the shielding is attained. The time scale for the shielding processes is typically less than 1 h [*Kikuchi et al.*, 2000; *Peymirat et al.*, 2000], but it depends on magnetospheric conditions [*Senior and Blanc*, 1984; *Maruyama et al.*, 2007]. During the main phase of a geomagnetic storm, the penetration electric field is sometimes observed to last for several hours without decay [*Kelley et al.*, 2003; *C.-S. Huang et al.*, 2005].

The ionospheric wind dynamo is an electrodynamic process that generates electric fields and currents as the electrically conducting atmosphere moves through the geomagnetic field [*Richmond*, 1995]. During a geomagnetic storm, the dynamo electric fields and currents are altered as the wind generated by high-latitude Joule heating and ion-drag forcing disturbs the normal quiet time thermospheric circulation. The theoretical basis of the storm time disturbance dynamo was established by *Blanc and Richmond* [1980]. The high-latitude forcing produces equatorward winds, which turns westward at middle and low latitudes due to the action of the Coriolis force. The westward wind drives equatorward currents, which build up positive charges near the equator. Poleward electric fields are thus set up, and they drive poleward Pedersen currents that substantially balance the wind driven equatorward currents. The poleward electric

fields also produce eastward Hall currents, which cause positive charge accumulation at the dusk terminator and negative charge accumulation at the dawn. The effect of the disturbance dynamo at equatorial latitudes is, therefore, a generation of a westward electric field on the dayside and eastward electric field on the nightside, which opposes the quiet time pattern. An additional mechanism was suggested by *Fuller-Rowell et al.* [2002], where storm time meridional wind surges drive eastward currents at middle latitudes, which would produce similar equatorial electric fields and currents as the *Blanc and Richmond* theory. This mechanism enables a rapid disturbance dynamo onset within an hour or two after the high-latitude energy input, because the slow buildup of westward winds due to the Coriolis force is not involved.

The low-latitude electrodynamic response to high-latitude geomagnetic activity has been extensively studied by B. G. Fejer and his colleagues using a large data set of vertical plasma drift measurements at Jicamarca (see reviews by *Fejer* [1981, 2002]). In particular, *Fejer and Scherliess* [1995, 1997] and *Scherliess and Fejer* [1997] introduced a technique to determine the average response of the equatorial vertical plasma drift to variable high-latitude forcing. By binning the data with respect to times of large increase or decrease in the auroral electrojet index *AE*, they were able to show how the disturbance electric field depends on the time history of auroral electrojet activity. Their approach was successful especially for the nighttime when disturbance signals were large. Daytime effects were, however, found to be small in the drift data, and the characteristics remained to be clarified.

Understanding the response of the daytime electric field to geomagnetic activity is important because it has a significant impact on the dayside ionospheric plasma distribution during geomagnetically disturbed periods [e.g., *Mannucci et al.*, 2005]. Ground-based magnetometer data have been often used to study the daytime equatorial electrojet response to geomagnetic activity. A number of case studies have been made to provide evidence for the effect of the prompt penetration electric field and disturbance dynamo electric field [e.g., *Sastri*, 1988; *Kikuchi et al.*, 2003, 2008; *Veenadhari et al.*, 2010; *Le Huy and Amory-Mazaudier*, 2005; *Zaka et al.*, 2009]. A weakness of case studies is that they do not consider the effect of quiet time day-to-day variations, which could be comparable to disturbance effects. The quiet time day-to-day variability of the equatorial electrojet arises primarily from irregular changes in the neutral wind caused by meteorological forcing from the lower atmosphere [*Yamazaki et al.*, 2014a]. The neglect of the quiet time variability is a significant issue particularly for the disturbance dynamo effect, which is usually identified by merely comparing the data for an event day against a reference quiet day. Meanwhile, a statistical approach such as work by *Fejer and Scherliess* [1995] has an advantage that it can average out the contribution of the quiet time variability by using a large data set. In the present study, we statistically analyze long-term records of geomagnetic data to reveal characteristics of the equatorial electrojet during periods of enhanced geomagnetic activity. The main objective is to establish the average (or climatological) response of the daytime equatorial electrojet to geomagnetic storms and substorms.

Geomagnetic storms and substorms are separate phenomena, involving different magnetospheric processes [e.g., *Kamide and Maltsev*, 2007]. Both phenomena are initiated by the injection of solar wind energy into the magnetosphere, and thus, they occur under similar solar wind conditions. As a result, almost all geomagnetic storms are accompanied by substorms, and most intense substorms occur during geomagnetic storms. Nonetheless, their behaviors are sometimes very different. For example, multiple (5–10) substorms with a period of 3–4 h are often observed during a single event of an intense geomagnetic storm [e.g., *Huang*, 2005; *Troshichev and Janzhura*, 2009]. The present study does not attempt to completely separate the contributions of the two phenomena, which would require a statistical analysis of storm events unaccompanied by a substorm as well as a statistical analysis of substorm events without a geomagnetic storm. Both geomagnetic storms and substorms involve enhanced energy input into the high-latitude thermosphere/ionosphere that affects the equatorial electrodynamics but they act on different time scales. A typical duration of a substorm is a few hours, while that of a geomagnetic storm is several hours to days. In this paper, the terms "geomagnetic storms" and "substorms" are used only to distinguish their time scales. For substorms, we investigate hour-to-hour responses between the *AE* index and equatorial electrojet perturbations. Meanwhile, for geomagnetic storms, responses between the disturbance storm time (*Dst*) index and equatorial electrojet perturbations are examined on the basis of a 6 h integration of data, which is longer than a typical duration of a substorm.

Table 1. Binning Criteria for Substorm Times t_1–t_8 and Average Indices (in nT) for the Indian Sector (*i*) and Peruvian Sector (*p*)

	AE_0	AE_1	AE_2	AE_3	$\lvert AE_0 - AE_1 \rvert$	Comments
t_1	>400	≤250	≤250	≤250	-	A sudden increase in auroral electrojet activity after at least 3 h of quiet period.
i	499.2	177.3	110.4	118.5		
p	501.7	176.2	108.3	117.0		
t_2	>400	>400	≤250	≤250	≤200	Two hours of high auroral electrojet activity with no large change during the last hour.
i	548.6	519.3	179.5	127.0		
p	548.2	521.7	177.2	124.9		
t_3	>400	>400	>400	≤250	≤200	Three hours of high auroral electrojet activity with no large change during the last hour.
i	607.7	635.4	520.2	185.4		
p	611.9	632.8	521.7	183.6		
t_4	>400	>400	>400	>400	≤200	At least 4 h of high auroral electrojet activity with no large change during the last hour.
i	653.8	666.1	686.4	675.8		
p	662.0	673.4	694.1	683.9		
t_5	≤250	>400	>400	>400	-	A sudden decrease in auroral electrojet activity after at least 3 h of active period.
i	189.3	519.0	658.2	614.5		
p	188.5	520.9	653.2	610.0		
t_6	≤250	≤250	>400	>400	-	Two hours of quiet geomagnetic condition after active period.
i	131.1	182.7	515.1	599.3		
p	128.1	183.1	516.4	594.0		
t_7	≤250	≤250	≤250	>400	-	Three hours of quiet geomagnetic condition after active period.
i	117.2	111.7	183.3	497.0		
p	113.8	110.5	182.2	498.3		
t_8	≤250	≤250	≤250	≤250	-	At least 4 h of quiet condition.
i	80.4	76.3	76.5	80.9		
p	80.9	76.6	76.8	81.3		

2. Data

We used hourly ground magnetometer data to derive the strength of the equatorial electrojet in the Indian and Peruvian regions. Following standard practice, a proxy for the equatorial electrojet intensity was obtained by taking the difference in the magnitudes of the horizontal (*H*) component of the geomagnetic field at a dip-equatorial station, where the dip latitude is within ±3° and an off-equatorial low-latitude station of the same longitude sector [e.g., *Rastogi*, 1989; *Anderson*, 2011]. This substantially removes the effect of magnetospheric currents from the data. The difference in *H* is denoted as ΔH. The baseline of ΔH was calculated as the average of the five-hourly nighttime values starting from midnight.

The pair of stations used in this study is Trivandrum (8.5°N, 77.0°E; 0.4°S dip) and Alibag (18.6°N, 72.9°E; 12.4°N dip) for the Indian sector from 1957 to 1998. The Trivandrum station closed in 1999, so that the data from Tirunelveli (8.7°N, 77.8°E) were used as a substitute from 1999 to 2011. The data from both Trivandrum and Tirunelveli were available from January to September 1999. During this period, *H* at the two stations showed nearly identical perturbations, which justifies the use of Tirunelveli as a replacement of Trivandrum from 1999 onward. After eliminating periods with no data, ΔH for the Indian sector covers 53 years in total. For the Peruvian sector, ΔH was calculated from *H* at Huancayo (12.0°S, 75.3°W; 0.9°N dip) and Fuquene (5.7°N, 73.7°W; 17.7°N dip). The Peruvian data set covers the years 1957–2007, but it suffers from a frequent lack of data, and the total available data are only for 22 years, which is less than half of the Indian data set.

We first determined the solar cycle, seasonal, lunar time, and local (solar) time-dependent quiet day ($Kp <= 2$) values $\Delta H_{\mathrm{Quiet}}$ using basically the methodology described by *Yamazaki et al.* [2011]. The $\Delta H_{\mathrm{Quiet}}$ is then subtracted from ΔH. The residuals $\Delta H - \Delta H_{\mathrm{Quiet}}$ are due to the effect of the prompt penetration electric field and disturbance dynamo electric field, as well as due to quiet time day-to-day variability. It is assumed that the quiet time day-to-day variations are independent of geomagnetic activity, while the variations due to the prompt penetration electric field and disturbance dynamo electric field depend on geomagnetic activity and its time history. Therefore, the quiet time day-to-day variations can be removed by averaging $\Delta H - \Delta H_{\mathrm{Quiet}}$ data under certain geomagnetic activity conditions.

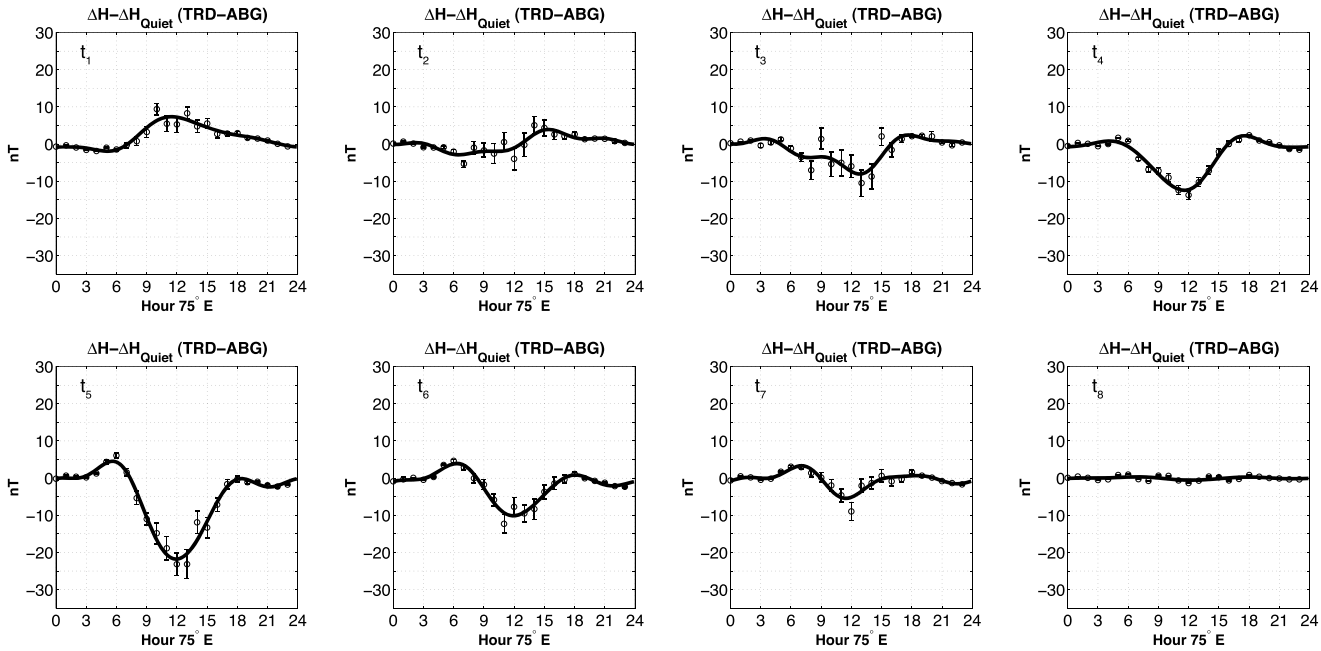

Figure 1. Equatorial electrojet perturbations in the Indian sector at the substorm times t_1–t_8 as defined in Table 1. The circles indicate the average value at each local time with error bars representing the standard error for the average. The solid curves show a smooth fit of a local time function as given by equation (1).

Hourly values of the *Dst* index and the *AE* index are used to quantify activities of geomagnetic storms and substorms, respectively. We use the corrected *Dst* index (or D_{cx}) given by *Mursula and Karinen* [2005].

3. Results and Discussion

3.1. Response to Substorms

The response of the equatorial electrojet to rapid changes in auroral electrojet activity was examined by binning the $\Delta H - \Delta H_{\text{Quiet}}$ data according to the time history of the hourly *AE* index, similar to the method introduced by *Fejer and Scherliess* [1995]. The binning criteria are given in Table 1, where AE_0 is the *AE* value for the present hour and AE_n ($n = 1, 2, 3$, or 4) is the *AE* value for n hours prior. The substorm times t_1–t_8 represent different stages of auroral electrojet activity, as indicated in Table 1.

Figure 1 illustrates the average response of the equatorial electrojet to auroral electrojet activity in the Indian sector. The eight panels show equatorial electrojet perturbations at substorm times t_1–t_8, which are defined in Table 1. In each panel, the circles indicate the average value of $\Delta H - \Delta H_{\text{Quiet}}$ at each local time. The error bars have a length of twice the standard error for the average. A smooth fit of a local time function is also indicated. The fitting function used is

$$f(t) = \sum_{k=0}^{4} \left[A_k \cos \frac{2\pi}{24} kt + B_k \sin \frac{2\pi}{24} kt \right], \tag{1}$$

where t is local time in hour and A_k and B_k are coefficients that can be determined by least squares fitting. The fitting was done to all the available data, not to the average data points at each local time.

The substorm time t_1 is when the *AE* index is suddenly increased after at least 3 h of quiet periods. It corresponds to substorm onset. (See Table 1 for the average *AE* indices for each substorm time.) Generally, the equatorial electric field perturbation after substorm onset could be either eastward or westward. *Huang* [2012] showed that the westward electric field perturbation is in many cases related to a northward turning of the interplanetary magnetic field (IMF), which often coincides with substorm onset. *Huang* [2012] also showed that the equatorial electric field perturbation after substorm onset is eastward when the IMF is continuously southward around the onset without a northward turning of the IMF. Our results for t_1 involve substorms both with and without a northward turning of the IMF. The results indicate that the average electrojet perturbation at substorm onset is dominated by an eastward electric field, which results from the prompt penetration of the dawn-to-dusk convection electric field to equatorial latitudes. The enhanced

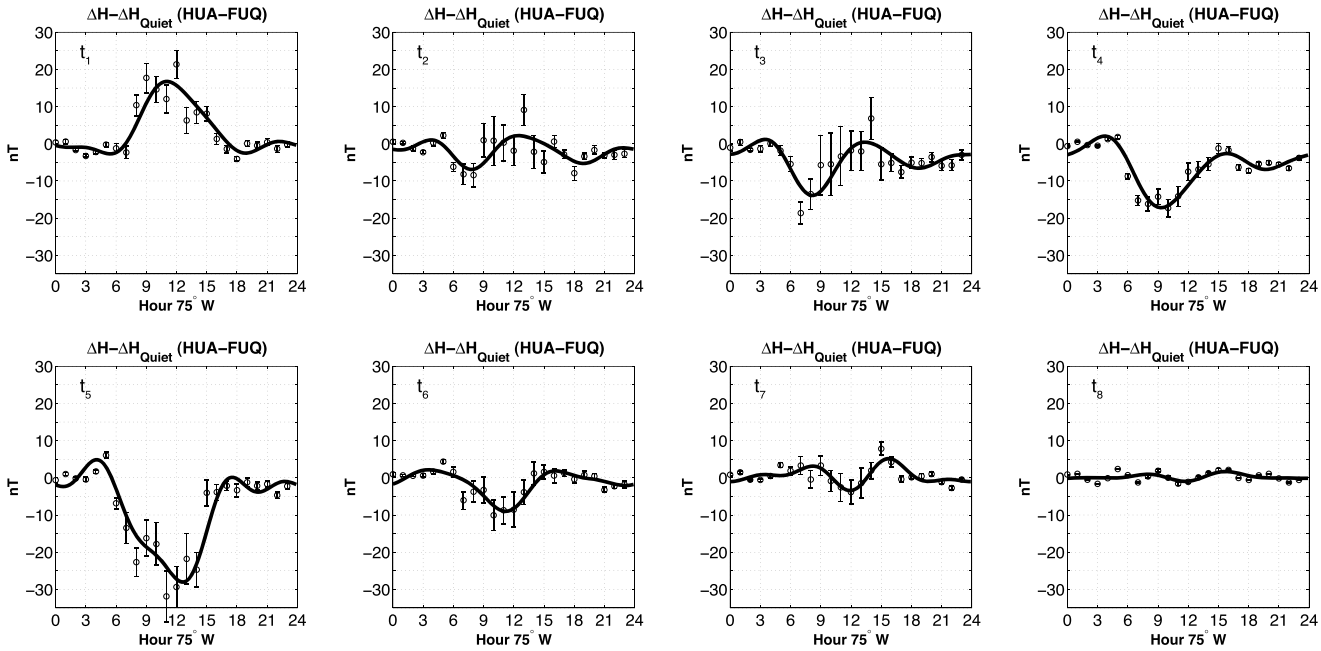

Figure 2. The same as Figure 1 but for the Peruvian sector.

eastward electric field fades away in 1 h, and a westward disturbance electrojet starts to dominate as geomagnetic activity remains high (t_2 and t_3). This decay of the eastward electrojet can be attributed to two processes. First, the development of the dusk-to-dawn shielding electric field reduces the effect of the dawn-to-dusk convection electric field. Second, a westward electric field due to the disturbance dynamo effect develops on the dayside low-latitude ionosphere.

The results for t_4 indicate that the westward disturbance electric field dominates when high auroral electrojet activity persists at least for four hours. Although the shielding process is completed at this stage, the enhanced high-latitude convection electric field leaks to lower latitudes and influences the equatorial electrojet. The westward disturbance electrojet at t_4 could be contributed by the eastward steady-state penetration electric field but be dominated by the westward disturbance dynamo electric field. The prompt penetration electric field under steady state conditions has been noticed in numerical simulations [*Peymirat et al.*, 2000; *Zaka et al.*, 2010], but often overlooked in interpreting observations. For example, *Fejer and Scherliess* [1995] and *Fejer et al.* [2008] attributed the disturbance electric field after four hours of high geomagnetic activity to the sole effect of the disturbance dynamo.

A sudden decrease in the *AE* index gives rise to a strong westward perturbation in the equatorial electrojet as indicated by the results at t_5. It is known that a rapid northward turning of the IMF from a steady southward condition, and thus a rapid substorm recovery, is often followed by a transient augmentation of the westward electric field at equatorial latitudes [e.g., *Rastogi and Patel*, 1975; *Fejer et al.*, 1979]. This is owing to the dusk-to-dawn shielding electric field that is left behind after the abrupt decrease of the dawn-to-dusk convection electric field [*Kelley et al.*, 1979]. The temporal progression from t_5 to t_7 demonstrates a gradual decay of the westward disturbance electrojet due to attenuation of both shielding electric field and disturbance dynamo electric field. The electrojet perturbation is negligible at t_8 after at least 4 h of quiet geomagnetic conditions.

Figure 2 shows the same as Figure 1, but for the Peruvian sector. The equatorial electrojet response to the changes in *AE* is largely consistent with the Indian sector results. Thus, our discussion on the Indian sector results is valid for the Peruvian sector results as well. The effect of the prompt penetration electric field at t_1 is larger in the Peruvian region than in the Indian region. This is probably because the effective ionospheric conductivity is greater in the Peruvian region due to weaker background geomagnetic field [*Shinbori et al.*, 2010].

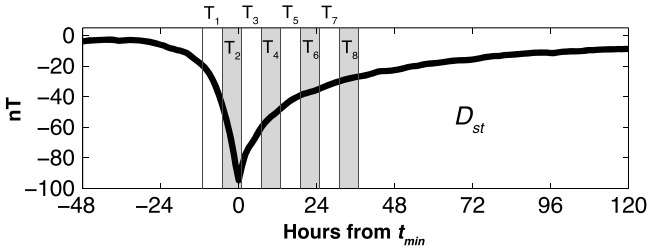

Figure 3. The average time series of the *Dst* index during geomagnetic storms over the period 1957–2011. Total 1324 storm events are included. Each event is required to have the minimum *Dst* less than −50 nT. The reference time t_{min} is the time when the *Dst* index reaches its minimum value for each storm event. Time intervals for the storm times T_1–T_8 are also indicated. T_n is defined as a 6 h interval from $6(n-3)+1+t_{min}$ to $6(n-2)+t_{min}$.

Substorm effects on the equatorial electrojet, presented in Figures 1 and 2, are consistent with what *Fejer and Scherliess* [1995] predicted on the basis of vertical plasma drift measurements at Jicamarca during 1968–1987. The present study involves more extensive data and examines magnetic signals of the equatorial electrojet, which is enhanced during the daytime due to increased ionospheric conductivities. Our results shed light on the daytime effect, which *Fejer and Scherliess* [1995] found difficult to clearly resolve in their data set. The results can be interpreted in terms of the penetration electric field and disturbance dynamo electric field, but it is difficult to know which is how much. We believe that our results at t_1–t_7 are more or less affected by both processes. The separation of the two contributions would be possible only through a comparison with numerical simulations that include both mechanisms.

3.2. Response to Geomagnetic Storms

For geomagnetic storm effects, ΔH–ΔH_{Quiet} were binned according to the time history of the hourly *Dst* index. All the storm events with the minimum *Dst* index less than −50 nT were identified for the period 1957–2011 (total 1324 storm events), and the time when the *Dst* reaches its minimum value was assigned as t_{min}. For multiple-onset storms, each phase with the minimum *Dst* index less than −50 nT was treated separately. Figure 3 shows the average time series of the *Dst* index as a function of time from t_{min}. The multiple-onset storms were carefully divided into pieces of events so that the same *Dst* value would not be used more than once in averaging. The results illustrate a typical geomagnetic storm with the main phase magnitude of $Dst(t_{min})=-94.7$ nT. The recovery phase can be recognized as a gradual recovery in *Dst* after the main phase. The storm onset, which is often characterized by a storm sudden commencement, is not visible in Figure 3. This is because the data were sorted with respect to t_{min}, not the onset time. Since we will focus on the equatorial electrojet response during the main phase and recovery phase, the exact time for the onset is not important for our results. We defined storm times T_1–T_8 according to the time with respect to t_{min}. T_n is a 6 h interval from $6(n-3)+1+t_{min}$ to $6(n-2)+t_{min}$, so that T_1 and T_2 are in the developing phase of the storm while T_3–T_8 are in the recovery phase. The time intervals for T_1–T_8 are indicated in Figure 3.

Figure 4 presents the response of the equatorial electrojet to geomagnetic storms in the Indian sector. Different panels show ΔH–ΔH_{Quiet} at different storm times T_1–T_8. (See Figure 3 for the time intervals for T_1–T_8.) The results demonstrate the development and decay of the electrojet perturbation during the average geomagnetic storm. The electrojet perturbation is mainly westward throughout the period we investigate. The westward disturbance in the equatorial electrojet persists for approximately 24 h after t_{min} (i.e., from T_3 to T_6). Such a long-lasting effect can result from the disturbance dynamo electric field, which has been predicted to last for many hours after high-latitude forcing ceases [*Blanc and Richmond*, 1980; *C.-M. Huang et al.*, 2005]. Indeed, in previous studies, equatorial electrojet perturbations during the recovery phase were often attributed to the disturbance dynamo effect [*Le Huy and Amory-Mazaudier*, 2005; *Zaka et al.*, 2009]. It should be noted, however, that we cannot rule out possible contributions of the steady-state penetration electric field that slowly attenuates during the recovery phase.

Figure 5 is the same as Figure 4 but for the Peruvian sector. The results for the Indian and Peruvian sectors show some similarities and differences. During the increase of storm activity at T_1 and T_2, a westward disturbance develops in both regions. Equatorial electrojet perturbations at T_1 and T_2 may include the contribution of short-term eastward penetration electric field but be dominated by the westward disturbance dynamo electric field. The local time for the maximum westward disturbance slightly shifts to later local times at the transition from the main phase to the recovery phase (i.e., from T_2 to T_3) in both Indian and Peruvian regions, which is probably due to changes in the penetration electric field from high

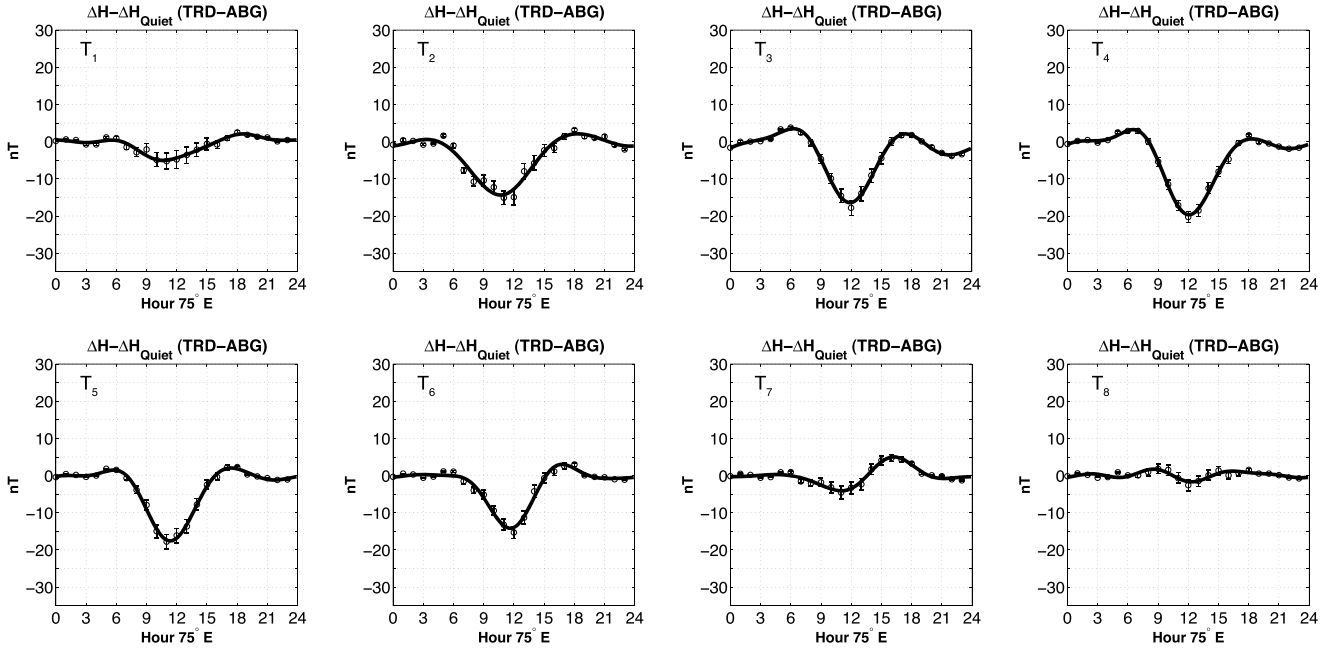

Figure 4. Equatorial electrojet perturbations in the Indian sector during geomagnetic storms. See Figure 3 for the storm times T_1–T_8. The results in each panel are shown in the same format as Figure 1.

latitudes. A marked difference in the results for the two regions is in the pattern of electrojet perturbations during the recovery phase. That is, the results for the Indian sector show a westward disturbance with a single peak around the noon, while the Peruvian sector results reveal a semidiurnal variation with a westward disturbance in the morning and eastward disturbance in the afternoon. The difference may result from a longitudinal dependence in the disturbance winds. The electrojet perturbation during the recovery phase persists for approximately 24 h in both regions. The duration of the effect (i.e., ~24 h) may be

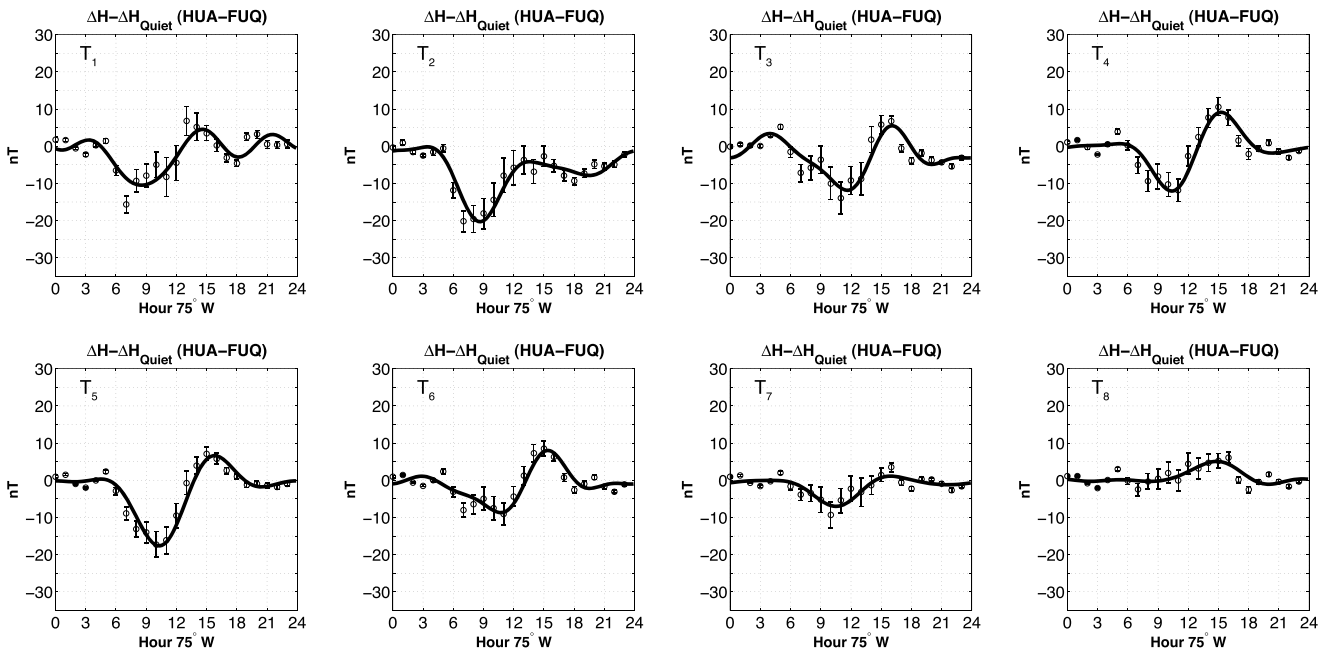

Figure 5. The same as Figure 4 but for the Peruvian sector.

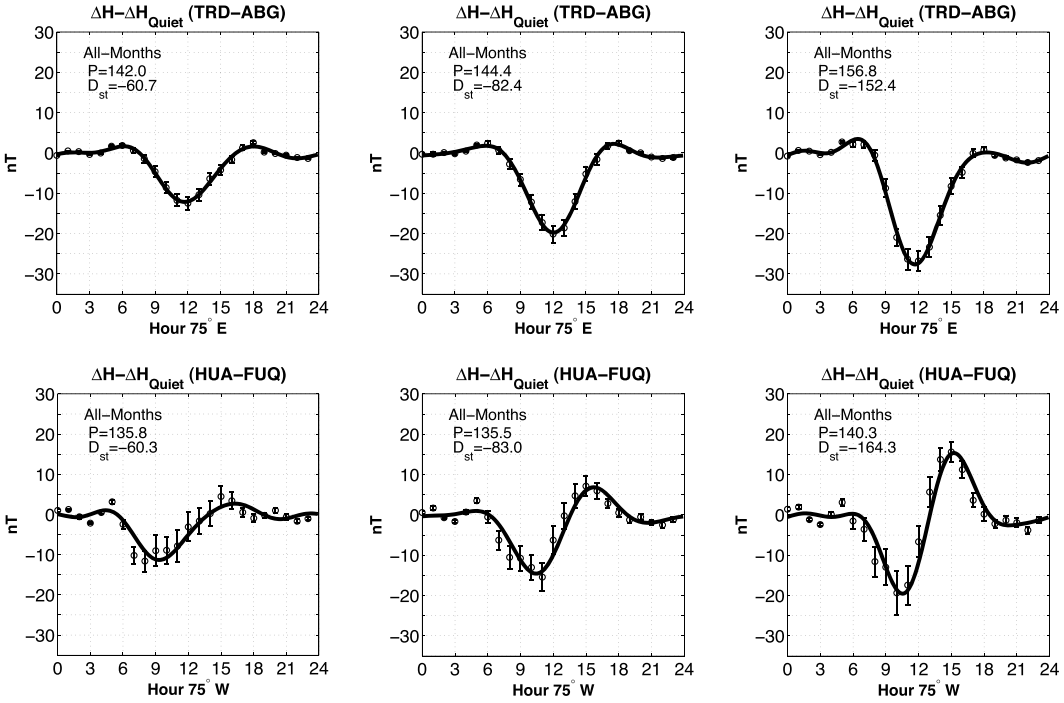

Figure 6. Equatorial electrojet perturbations during the recovery phase of geomagnetic storms (T_4 and T_5) for (left) weak, (middle) moderate, and (right) strong storms. The top and bottom show the results for the Indian and Peruvian sectors, respectively. The results in each panel are shown in the same format as Figure 1, except that the average solar activity index *P* and minimum *Dst* index are also indicated.

dependent on the magnitude of the storm. Thus, it should not be considered as a solid number but should be interpreted as a typical time scale for an average storm.

We now take a closer look at the "after-storm" effect, which is evident during the recovery phase. The results for T_4 and T_5 are combined at each longitude sector, and regrouped according to the magnitude of the storm, solar EUV activity, and season. Concretely, the storm magnitude binning is based on the *Dst* value at t_{min} (i.e., the minimum *Dst* value), and binning criteria are $Dst(t_{min}) > -70$ nT for weak storms; $-100 < Dst(t_{min}) \leq -70$ nT for moderate storms; and $Dst(t_{min}) \leq -100$ nT for strong storms. For the solar EUV activity binning, we use the index *P* [*Richards et al.*, 1994], which is defined as the average of the daily $F_{10.7}$ index and its 81 day mean. The binning criteria are $P \leq 80$ sfu, $80 < P \leq 180$ sfu, $P > 180$ sfu, where sfu denotes the solar flux unit, 10^{-22} W m^{-2} Hz^{-1}. The seasonal binning is based on the three Lloyd seasons, i.e., D months consisting of November, December, January, and February; E months consisting of March, April, September, and October; and J months consisting of May, June, July, and August.

Figure 6 depicts how the electrojet perturbation during the recovery phase depends on the magnitude of the storm. The results indicate that a larger storm leads to a stronger effect. In the Peruvian sector, not only the westward disturbance in the morning but also the eastward disturbance in the afternoon increases with increasing storm intensity. A larger storm involves more energy input to the high-latitude upper atmosphere, which would drive stronger and longer-lasting disturbance winds and resulting disturbance dynamo electric field.

Figure 7 shows equatorial electrojet perturbations during the recovery phase for different solar EUV activity conditions. The after-storm effect tends to be more significant for higher solar activity. This is probably due to enhanced ionospheric conductivities during high solar flux periods. For quiet conditions, daytime ionospheric dynamo currents are approximately twice as strong during solar maximum in comparison with solar minimum [e.g., *Takeda*, 1999, 2002]. Besides, numerical experiments by *Huang* [2013] showed that the disturbance dynamo electric field is stronger for higher solar flux conditions for the same storm, although the mechanism was not examined.

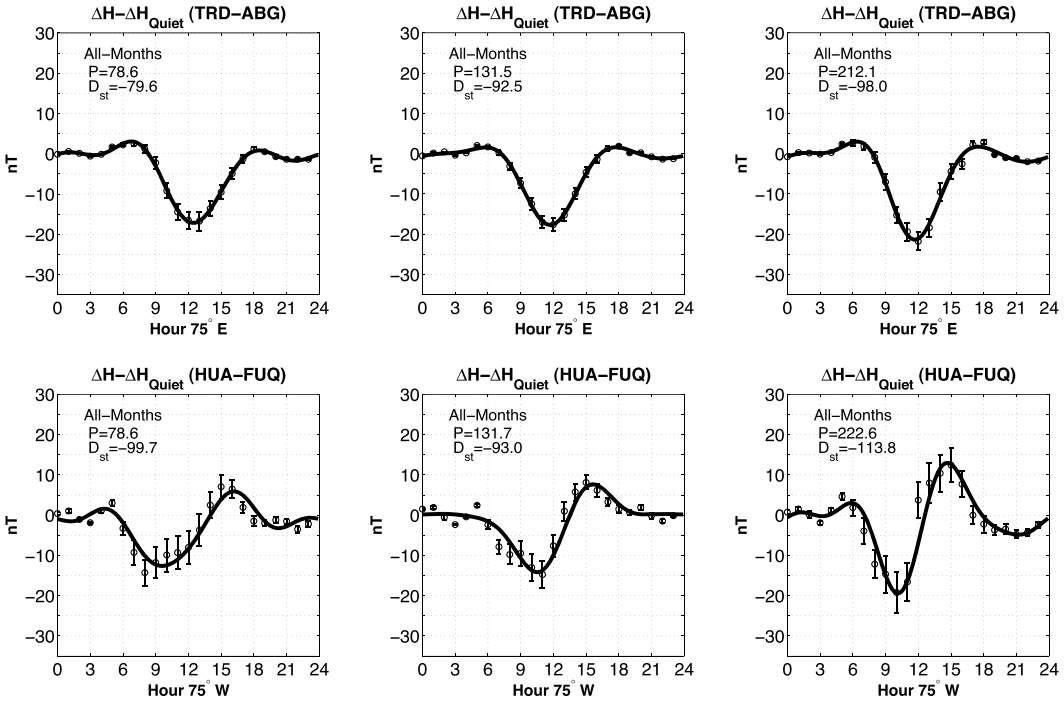

Figure 7. Equatorial electrojet perturbations during the recovery phase of geomagnetic storms (T_4 and T_5) for (left) low, (middle) moderate, and (right) high solar EUV activity. The results are shown in the same format as Figure 6.

Seasonal effects, presented in Figure 8, reveal longitudinal differences. In the Indian sector, the westward disturbance shows a strong annual modulation with maximum effect during the D months and minimum effect during the J months. The seasonal variation is barely visible in the Peruvian sector results, except that the eastward disturbance in the afternoon is largest during the D months. It is probable that storm-time

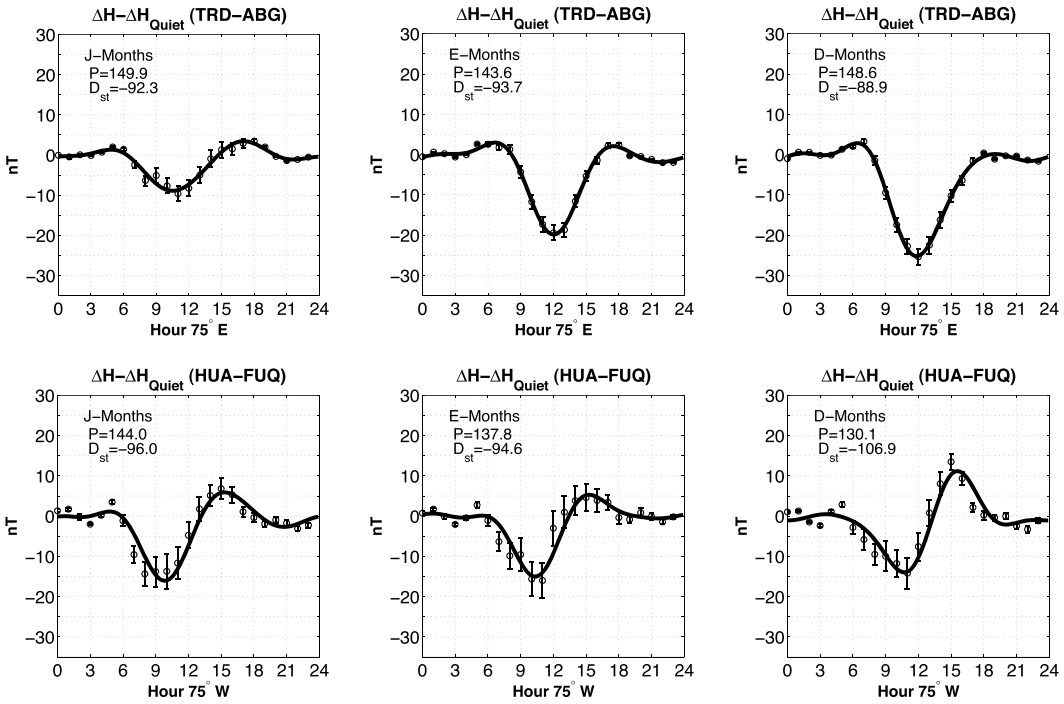

Figure 8. Equatorial electrojet perturbations during the recovery phase of geomagnetic storms (T_4 and T_5) for (left) J months, (middle) E months, and (right) D months. The results are shown in the same format as Figure 6.

disturbance winds vary with the season, so that the resulting disturbance dynamo electric field is also seasonal dependent. The dependence of disturbance winds on the season is not well understood. The most comprehensive empirical model, DWM07 [*Emmert et al.*, 2008], does not include seasonal variations. Further studies will be required in order to understand the seasonal dependence of the disturbance equatorial electrojet, presented in Figure 8. It may be noted that the equatorial electrojet flows in the Northern Hemisphere at the Indian sector, while the Peruvian electrojet flows in the Southern Hemisphere. Such a difference in geographical conditions adds to the complexity in how the disturbance dynamo electric field changes with season at different longitudes.

It is interesting that the results for the J months show a semidiurnal perturbation in both regions, i.e., a westward disturbance in the morning and an eastward disturbance in the afternoon. A semidiurnal perturbation in the quiet time equatorial electrojet is often a manifestation of semidiurnal tidal forcing from the lower atmosphere [e.g., *Yamazaki et al.*, 2014b]. It may be possible that the upward propagating semidiurnal tides are altered during geomagnetic storms due to changes in the background thermospheric wind. The feasibility of this mechanism is yet to be studied.

4. Summary

Using long time series of ground magnetic field measurements, we have examined the climatology of the equatorial electrojet response to geomagnetic storms and substorms in the Indian and Peruvian sectors. Substorm effects have been determined by sorting the equatorial electrojet perturbations according to the time history of the *AE* index. It has been shown that a sudden increase in the *AE* index leads to an enhancement of the daytime eastward electrojet, indicating the penetration of the high-latitude convection electric field to lower latitudes. The enhanced eastward electrojet fades away in 1 h, and as geomagnetic activity remains high, a westward disturbance electrojet starts to dominate, which is a manifestation of the disturbance dynamo electric field. A rapid reduction in *AE* is followed by an intensification of the westward disturbance electrojet, which can be attributed to the dusk-to-dawn shielding electric field. These results are in good agreement with previous studies based on *F* region equatorial vertical plasma drift measurements [e.g., *Fejer and Scherliess*, 1995].

Storm effects have been examined by arranging equatorial electrojet perturbations with respect to the time for the minimum *Dst*. The disturbance electrojet develops as the storm intensifies, and it persists for approximately 24 h during the recovery phase for the average storm with the minimum *Dst* value of −94.7 nT. The electrojet perturbations during the recovery phase are likely to be due to the disturbance dynamo electric field, which has been predicted to last for many hours after geomagnetic activity subsides [*Blanc and Richmond*, 1980; *Huang et al.*, 2005]. In the Indian sector, the after-storm effect is characterized by a westward disturbance with a maximum around the noon, while in the Peruvian sector, the effect is more semidiurnal with a westward disturbance in the morning and an eastward disturbance in the afternoon. Further analysis has revealed that the after-storm effect is dependent on the magnitude of the storm, solar EUV activity, and season. That is, the amplitude of the electrojet perturbations during the recovery phase tends to increase with an increase in the storm magnitude and solar flux level. The after-storm effect in the Indian sector shows a strong annual modulation with maximum and minimum effects during northern winter and summer, respectively. Meanwhile, the seasonal variation is not so apparent in the Peruvian sector.

Acknowledgments

We thank A.D. Richmond for reviewing a draft manuscript and for insightful comments and suggestions. Hourly geomagnetic data were obtained from the World Data Centre for Geomagnetism (Edinburgh) website at http://wdc.bgs.ac.uk. The *AE* index was downloaded from the World Data Centre for Geomagnetism (Kyoto) website at http://wdc.kugi.kyoto-u.ac.jp. The corrected *Dst* index, or D_{cx}, was provided by the University of Oulu, Finland, at http://dcx.oulu.fi. The *Kp* index was provided by the German Research Center for Geosciences (GFZ). The solar activity index $F_{10.7}$ was provided by the Herzberg Institute of Astrophysics. This work was supported by NERC grant NE/K01207X/1.

Alan Rodger thanks the reviewers for their assistance in evaluating this paper.

References

Anderson, D. (2011), Daytime vertical E×B drift velocities inferred from ground-based equatorial magnetometer observations, in *Aeronomy of the Earth's Atmosphere and Ionosphere*, vol. 2, edited by M. A. Abdu, D. Pancheva, and A. Bhattacharyya, pp. 203–210, Springer, Netherlands, doi:10.1007/978-94-007-0326-1.

Blanc, M., and A. D. Richmond (1980), The ionospheric disturbance dynamo, *J. Geophys. Res.*, *85*(A4), 1669–1686, doi:10.1029/JA085iA04p01669.

Emmert, J. T., D. P. Drob, G. G. Shepherd, G. Hernandez, M. J. Jarvis, J. W. Meriwether, R. J. Niciejewski, D. P. Sipler, and C. A. Tepley (2008), DWM07 global empirical model of upper thermospheric storm-induced disturbance winds, *J. Geophys. Res.*, *113*, A11319, doi:10.1029/2008JA013541.

Fejer, B. G. (1981), The equatorial ionospheric electric field. A review, *J. Atmos. Terr. Phys.*, *43*, 377–386.

Fejer, B. G. (2002), Low latitude storm time ionospheric electrodynamics, *J. Atmos. Sol. Terr. Phys.*, *64*, 1401–1408.

Fejer, B. G., and L. Scherliess (1995), Time-dependent response of equatorial ionospheric electric fields to magnetospheric disturbances, *Geophys. Res. Lett.*, *22*, 851–854, doi:10.1029/95GL00390.

Fejer, B. G., and L. Scherliess (1997), Empirical models of storm time equatorial zonal electric fields, *J. Geophys. Res.*, *102*(A11), 24,047–24,056, doi:10.1029/97JA02164.

Fejer, B., C. Gonzales, D. Farley, M. Kelley, and R. Woodman (1979), Equatorial electric fields during magnetically disturbed conditions: 1. The effect of the interplanetary magnetic field, *J. Geophys. Res.*, *84*(A10), 5797–5802, doi:10.1029/JA084iA10p05797.

Fejer, B. G., J. W. Jensen, and S.-Y. Su (2008), Seasonal and longitudinal dependence of equatorial disturbance vertical plasma drifts, *Geophys. Res. Lett.*, *35*, L20106, doi:10.1029/2008GL035584.

Fuller-Rowell, T. J., G. H. Millward, A. D. Richmond, and M. V. Codrescu (2002), Storm-time changes in the upper atmosphere at low latitudes, *J. Atmos. Sol.-Terr. Phys.*, *64*, 1383–1391.

Gonzales, C., M. Kelley, B. Fejer, J. Vickrey, and R. Woodman (1979), Equatorial electric fields during magnetically disturbed conditions: 2. Implications of simultaneous auroral and equatorial measurements, *J. Geophys. Res.*, *84*(A10), 5803–5812, doi:10.1029/JA084iA10p05803.

Huang, C.-M. (2013), Disturbance dynamo electric fields in response to geomagnetic storms occurring at different universal times, *J. Geophys. Res. Space Physics*, *118*, 496–501, doi:10.1029/2012JA018118.

Huang, C.-M., A. D. Richmond, and M.-Q. Chen (2005), Theoretical effects of geomagnetic activity on low-latitude ionospheric electric fields, *J. Geophys. Res.*, *110*, A05312, doi:10.1029/2004JA010994.

Huang, C.-S. (2005), Variations of polar cap index in response to solar wind changes and magnetospheric substorms, *J. Geophys. Res.*, *110*, A01203, doi:10.1029/2004JA010616.

Huang, C.-S. (2012), Statistical analysis of dayside equatorial ionospheric electric fields and electrojet currents produced by magnetospheric substorms during sawtooth events, *J. Geophys. Res.*, *117*, A02316, doi:10.1029/2011JA017398.

Huang, C.-S., J. C. Foster, and M. C. Kelley (2005), Long-duration penetration of the interplanetary electric field to the low-latitude ionosphere during the main phase of magnetic storms, *J. Geophys. Res.*, *110*, A11309, doi:10.1029/2005JA011202.

Kamide, Y., and Y. P. Maltsev (2007), Geomagnetic storms, in *Handbook of the Solar-Terrestrial Environment*, edited by Y. Kamide, and A. Chian, pp. 355–374, Springer, Berlin, doi:10.1007/11367758_14, (to appear in print).

Kelley, M. C., B. G. Fejer, and C. A. Gonzales (1979), An explanation for anomalous equatorial ionospheric electric fields associated with a northward turning of the interplanetary magnetic field, *Geophys. Res. Lett.*, *6*, 301–304, doi:10.1029/GL006i004p00301.

Kelley, M. C., J. J. Makela, J. L. Chau, and M. J. Nicolls (2003), Penetration of the solar wind electric field into the magnetosphere/ionosphere system, *Geophys. Res. Lett.*, *30*(4), 1158, doi:10.1029/2002GL016321.

Kikuchi, T., H. Lühr, K. Schlegel, H. Tachihara, M. Shinohara, and T.-I. Kitamura (2000), Penetration of auroral electric fields to the equator during a substorm, *J. Geophys. Res.*, *105*(A10), 23,251–23,261, doi:10.1029/2000JA900016.

Kikuchi, T., K. K. Hashimoto, T.-I. Kitamura, H. Tachihara, and B. Fejer (2003), Equatorial counterelectrojets during substorms, *J. Geophys. Res.*, *108*(A11), 1406, doi:10.1029/2003JA009915.

Kikuchi, T., K. K. Hashimoto, and K. Nozaki (2008), Penetration of magnetospheric electric fields to the equator during a geomagnetic storm, *J. Geophys. Res.*, *113*, A06214, doi:10.1029/2007JA012628.

Le Huy, M., and C. Amory-Mazaudier (2005), Magnetic signature of the ionospheric disturbance dynamo at equatorial latitudes: "D_{dyn}", *J. Geophys. Res.*, *110*, A10301, doi:10.1029/2004JA010578.

Mannucci, A. J., B. T. Tsurutani, B. A. Iijima, A. Komjathy, A. Saito, W. D. Gonzalez, F. L. Guarnieri, J. U. Kozyra, and R. Skoug (2005), Dayside global ionospheric response to the major interplanetary events of October 29–30, 2003 Halloween Storms, *Geophys. Res. Lett.*, *32*, L12S02, doi:10.1029/2004GL021467.

Maruyama, N., A. D. Richmond, T. J. Fuller-Rowell, M. V. Codrescu, S. Sazykin, F. R. Toffoletto, R. W. Spiro, and G. H. Millward (2005), Interaction between direct penetration and disturbance dynamo electric fields in the storm-time equatorial ionosphere, *Geophys. Res. Lett.*, *32*, L17105, doi:10.1029/2005GL023763.

Maruyama, N., S. Sazykin, R. W. Spiro, D. Anderson, A. Anghel, R. A. Wolf, F. R. Toffoletto, T. J. Fuller-Rowell, M. V. Codrescu, and A. D. Richmond (2007), Modeling storm-time electrodynamics of the low-latitude ionosphere-thermosphere system: Can long lasting disturbance electric fields be accounted for?, *J. Atmos. Sol. Terr. Phys.*, *69*, 1182–1199.

Mursula, K., and A. Karinen (2005), Explaining and correcting the excessive semiannual variation in the *Dst* index, *Geophys. Res. Lett.*, *32*, L14107, doi:10.1029/2005GL023132.

Nishida, A. (1968), Coherence of DP 2 fluctuations with interplanetary magnetic field variations, *J. Geophys. Res.*, *73*, 5549–5559.

Peymirat, C., A. D. Richmond, and A. T. Kobea (2000), Electrodynamic coupling of high and low latitudes: Simulations of shielding/overshielding effects, *J. Geophys. Res.*, *105*(A10), 22,991–23,003, doi:10.1029/2000JA000057.

Rastogi, R. G. (1989), The equatorial electrojet: Magnetic and ionospheric effects, in *Geomagnetism*, vol. 3, edited by J. Jacobs, pp. 461–525, Academic, New York.

Rastogi, R. G., and V. L. Patel (1975), Effect of interplanetary magnetic field on ionosphere over the magnetic equator, *Proc. Indian Acad. Sci.*, *82*, 121–141.

Richards, P. G., J. A. Fennelly, and D. G. Torr (1994), EUVAC: A solar EUV flux model for aeronomic calculations, *J. Geophys. Res.*, *99*(A5), 8981–8992, doi:10.1029/94JA00518.

Richmond, A. D. (1995), Ionospheric electrodynamics, in *Handbook of Atmospheric Electrodynamics*, vol. 2, edited by H. Volland, pp. 249–290, CRC Press, Boca Raton, Fla.

Richmond, A. D., C. Peymirat, and R. G. Roble (2003), Long-lasting disturbances in the equatorial ionospheric electric field simulated with a coupled magnetosphere-ionosphere-thermosphere model, *J. Geophys. Res.*, *108*(A3), 1118, doi:10.1029/2002JA009758.

Sastri, H. (1988), Equatorial electric field of ionospheric disturbance dynamo origin, *Ann. Geophys.*, *6*, 635–642.

Scherliess, L., and B. G. Fejer (1997), Storm time dependence of equatorial disturbance dynamo zonal electric fields, *J. Geophys. Res.*, *102*(A11), 24,037–24,046, doi:10.1029/97JA02165.

Senior, C., and M. Blanc (1984), On the control of magnetospheric convection by the spatial distribution of ionospheric conductivities, *J. Geophys. Res.*, *89*(A1), 261–284, doi:10.1029/JA089iA01p00261.

Shinbori, A., et al. (2010), Anomalous occurrence features of the preliminary impulse of geomagnetic sudden commencement in the South Atlantic Anomaly region, *J. Geophys. Res.*, *115*, A08309, doi:10.1029/2009JA015035.

Takeda, M. (1999), Time variation of global geomagnetic S_q field in 1964 and 1980, *J. Atmos. Sol. Terr. Phys.*, *61*, 765–774.

Takeda, M. (2002), Features of global geomagnetic S_q field from 1980 to 1990, *J. Geophys. Res.*, *107*(A9), 1252, doi:10.1029/2001JA009210.

Troshichev, O., and A. Janzhura (2009), Relationship between the PC and AL indices during repetitive bay-like magnetic disturbances in the auroral zone, *J. Atmos. Sol. Terr. Phys.*, *71*, 1340–1352, doi:10.1016/j.jastp.2009.05.017.

Veenadhari, B., S. Alex, T. Kikuchi, A. Shinbori, R. Singh, and E. Chandrasekhar (2010), Penetration of magnetospheric electric fields to the equator and their effects on the low-latitude ionosphere during intense geomagnetic storms, *J. Geophys. Res.*, *115*, A03305, doi:10.1029/2009JA014562.

Wolf, R. A. (1995), Magnetospheric configuration, in *Introduction to Space Physics*, edited by M. G. Kivelson, and C. T. Russell, pp. 288–329, Cambridge Univ. Press, New York.

Yamazaki, Y., et al. (2011), An empirical model of the quiet daily geomagnetic field variation, *J. Geophys. Res.*, *116*, A10312, doi:10.1029/2011JA016487.

Yamazaki, Y., A. D. Richmond, A. Maute, H.-L. Liu, N. Pedatella, and F. Sassi (2014a), On the day-to-day variation of the equatorial electrojet during quiet periods, *J. Geophys. Res. Space Physics*, *119*, 6966–6980, doi:10.1002/2014JA020243.

Yamazaki, Y., A. D. Richmond, A. Maute, Q. Wu, D. A. Ortland, A. Yoshikawa, I. A. Adimula, B. Rabiu, M. Kunitake, and T. Tsugawa (2014b), Ground magnetic effects of the equatorial electrojet simulated by the TIE-GCM driven by TIMED satellite data, *J. Geophys. Res. Space Physics*, *119*, 3150–3161, doi:10.1002/2013JA019487.

Zaka, K. Z., A. T. Kobea, P. Assamoi, K. O. Obrou, V. Doumbia, K. Boka, B. J.-P. Adohi, and N. M. Mene (2009), Latitudinal profile of the ionospheric disturbance dynamo magnetic signature: Comparison with the DP2 magnetic disturbance, *Ann. Geophys.*, *27*, 3523–3536.

Zaka, K. Z., et al. (2010), Simulation of electric field and current during the 11 June 1993 disturbance dynamo event: Comparison with the observations, *J. Geophys. Res.*, *115*, A11307, doi:10.1029/2010JA015417.